ridge. Perturbational model parameters, assigned separately from the ray-tracing model, were at horizontal and vertical nodal spacings of 20 and 25 km, respectively. The inverse problem was regularized by minimizing a stochastic penalty function and the model roughness. Results presented here were heavily smoothed (half-width of the Gaussian-shaped smoothing function was equal to the perturbational nodal spacing) and "squeezed" so that model perturbations were confined to depths less than a squeezing depth Z_s. The squeezing was implemented by assuming prior uncertainties of 10% and 0.01% in velocity above and below Z_s, respectively.

12. Synthetic data for each type of body wave were calculated for a ray set identical to that used in the inversion of actual data. Gaussian noise with a standard deviation of 0.1 s and 0.3 s was added to the synthetic *P* and *S* wave data, respectively.
13. S. Karato, *Geophys. Res. Lett.* **20**, 1623 (1993).
14. M. K. McNutt and A. V. Judge, *Science* **248**, 969 (1990).
15. J. R. Cochran, *Geophys. J. R. Astron. Soc.* **87**, 421 (1986); M. A. Eberle, D. W. Forsyth, E. M. Parmentier, *J. Geophys. Res.*, in press.
16. H. Schmeling, *Phys. Earth Planet. Inter.* **41**, 34 (1985); U. H. Faul, D. R. Toomey, H. S. Waff, *Geophys. Res. Lett.* **21**, 29 (1994).
17. D. W. Forsyth, in *Mantle Flow and Melt Generation at Mid-Ocean Ridges,* J. Phipps Morgan, D. K. Blackman, J. M. Sinton, Eds., vol. 71 of *Geophysical Monograph Series* (American Geophysical Union, Washington, DC, 1992), p. 1.
18. D. K. Blackman, J. A. Orcutt, D. W. Forsyth, J.-M. Kendall, *Nature* **366**, 675 (1993).
19. S. Stein, H. J. Melosh, J. B. Minster, *Earth Planet. Sci. Lett.* **36**, 51 (1977); H. Schouten, H. J. B. Dick, K. D. Klitgord, *Nature* **326**, 835 (1987).

20. D. W. Forsyth and C. J. Wolfe provided helpful comments. Supported by the Ocean Sciences Division of NSF.

12 February 1998; accepted 21 April 1998

Structure of the Upper Mantle Under the EPR from Waveform Inversion of Regional Events

Spahr C. Webb* and Donald W. Forsyth

Waveform inversions of seismograms recorded at the Mantle Electromagnetic and Tomography (MELT) Experiment ocean bottom seismometer array from regional events with paths following the East Pacific Rise (EPR) require that low shear velocities (<3.7 km/s) extend to depths of more than 100 km below the rise axis. Velocities increase with average crustal age along ray paths. The reconciliation of Love and Rayleigh wave data requires that shear flow has aligned melt pockets or olivine crystals, creating an anisotropic uppermost mantle.

Earthquakes on transform faults along the EPR during the 6-month-long deployment of ocean bottom seismometers (OBSs) of the MELT Experiment provided ray paths that closely follow the ridge crest and allowed direct observation of near-axis, upper mantle structure (Fig. 1). Previous models of ridge crest upper mantle structure (*1–3*) derived with surface wave observations from land have been limited in horizontal resolution to scales of 1000 km or more (*4*).

Three transform earthquakes on the EPR provided good records at the ocean bottom array (Fig. 1). Noise levels varied substantially across the array, reflecting differences among instruments and between sites. We selected a subset of the MELT array waveforms with good signal-to-noise ratios (SNRs) for each event (*5*). Horizontal component noise levels were higher and more variable than vertical noise levels because of current-induced tilt noise, but good-quality horizontal records were obtained on a small subset of the array (Fig. 2).

The vertical waveforms include both Rayleigh surface waves and *S* phases that are polarized with a radial and vertical component (SV). These waves were also recorded on the radial component of horizontal motion, but we used only the vertical component because the SNR was better. Rayleigh wave velocities depend on density and both compressional and shear velocity, but the primary sensitivity is equivalent to that of a vertically polarized, horizontal traveling *S* wave (*6*). Love surface waves and the horizontal (SH) component of *S* phases are polarized so that they are transverse to the direction of propagation and can be detected only on the noisier, horizontal components (*5*).

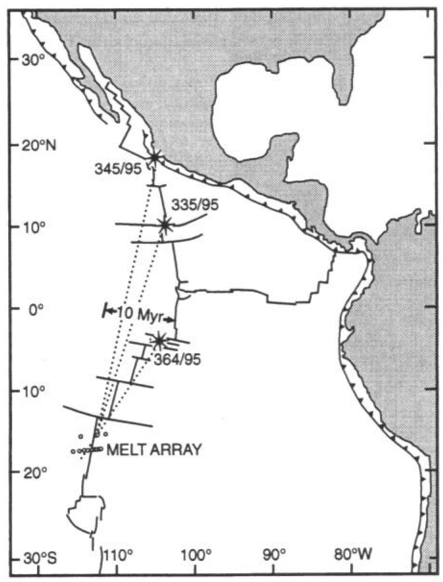

Fig. 1. Location of the three regional events along the EPR and the MELT Experiment OBSs used in this study. Approximate ray paths are shown.

Wave speeds in mantle rocks are anisotropic; shear and compressional wave velocities depend on the direction of travel, and shear wave velocities depend on the sense of polarization. The effects of weak anisotropy result in an apparently different model for shear wave velocities for the Love wave measurements than for the Rayleigh wave observations. The ratio of the shear velocities in the two models provides an estimate of the anisotropic component, although in strongly anisotropic material, Love and Rayleigh wave data are better modeled as coupled modes (*7, 8*).

We fit the observed waveforms to synthetic seismograms calculated for laterally homogeneous models with a reflectivity code (*9*) modified by the incorporation of the instrument responses into the code. We applied a bandpass filter (0.008 to 0.06 Hz) to suppress the long-period noise and the short-period Rayleigh waves strongly affected by multipathing and horizontal refraction (*10*). The OBS instrument response in this band is proportional to acceleration (*11*). Models were iteratively modified to best fit the data with the use linear inverse

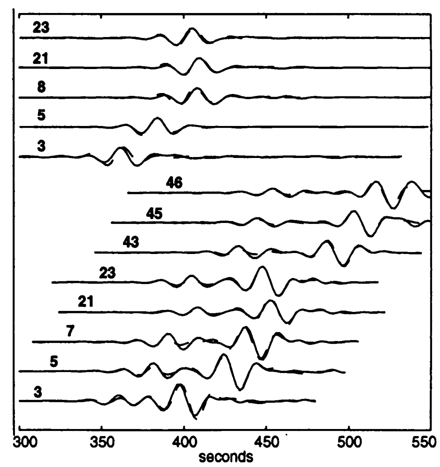

Fig. 2. Love wave (tangential component, top five traces) records and Rayleigh wave (vertical component, bottom eight traces) records for the 364/95 event, with synthetic seismogram fits based on the models shown in Fig. 3. Site number is shown for each trace.

S. C. Webb, Scripps Institution of Oceanography, University of California, San Diego, La Jolla, CA 92093, USA.
D. W. Forsyth, Department of Geological Science, Brown University, Providence, RI 02912, USA.

*To whom correspondence should be addressed at scwebb@ucsd.edu

theory with a smoothing constraint in the vertical (*12*). The reflectivity code models both the body wave (*P* and *S* waves) and surface wave data. This is necessary because the shear wave and surface wave arrivals at regional distances are not substantially separated in time. Modeling body waves and surface waves together provides stronger constraints on upper mantle structure than can be obtained from the analysis of surface wave data alone. The inversion scheme used calculations of the change in the synthetic waveform with changes in model parameter (synthetic derivatives) to make changes in the starting model to best fit the observed waveforms. Groups of OBS records from each event were fit to obtain estimates of the average Earth model between the event and the array.

Event locations and mechanisms were obtained from the Harvard CMT catalog (*13*). Errors in the models associated with event mislocation and origin time should be less than 0.5 % (root mean square). The ray paths from an event (364/95) on the Gofar transform fault lie solely under ocean crust less than 2 million years old (Fig. 1). The structure determined from these waveforms gives an unambiguous picture of the structure directly under the rise axis. We fit the vertical component waveforms from eight OBSs for this event with three models to account for the lateral variations in structure across the array and between the array and the source (Fig. 3). The subtle variations in velocities between the models are primarily required to account for the lateral variations in shallow structure in the vicinity of the array.

The shear wave velocities (SV) found for the 364/95 event (<3.7 km/s) in the low-velocity zone (LVZ) are considerably lower than previous estimates of shear velocity in the LVZ based on data from land stations but are similar to results from the Lau and Fiji basins obtained by applying a similar technique to regional data from island stations (*12*, *14*). A progression in the shear velocity in the LVZ and in the overlying lid (the higher velocity lithosphere) is evident in the models for the three events that involve ray paths traveling on progressively older average age crust (Fig. 4). These observations are consistent with a thickening lithosphere as the plate cools away from the rise axis but require a broad LVZ under the rise axis.

An analysis of the expected change in the model due to a small change in the true Earth model at different depths ("the resolution kernels") reveals the usefulness of each data set for constraining structure in the upper mantle (Fig. 5). The structure in the upper 100 km from all three events is well constrained by the amplitude and phase of the Rayleigh wave train (the last set of arrivals in each record), but the vertical resolution from surface waves alone becomes poor below 125 km. Body waves provide additional constraints on deeper structure for the 364/95 event down to about 200 km. The structure between 200 and 300 km is only weakly resolved because no arrivals turn in this depth range with nearly constant velocity. The deeper structure for the SV for the 364/95 event model is constrained by body waves turning just above the 410-km discontinuity. There is no indication of delays for waves bottoming near 410 km caused by anomalous structure between 200 and 410 km. If the shear velocity is assumed to be a monotonically increasing function of depth in this depth range, velocities between 200 and 300 km are restricted to lie between about 4.4 and 4.6 km/s, consistent with previous models derived from Rayleigh wave observations (*1*, *15*, *16*). The two other events have a larger gap in resolution between the upper 125 km constrained by Rayleigh waves and structure near the 410-km discontinuity controlled by body waves, so the models in Fig. 4 are restricted to vary only in the upper 125 km. The vertical waveforms can be fit with the bottom of the LVZ 25 km shallower, but the SH (Love) data from the 364/95 event require the deeper transition shown (Fig. 3). The SH waveforms (Fig. 2) require a pronounced shear velocity minimum at a depth of about 100 km, which pushes the LVZ deeper unless the sense of the SH-SV discrepancy changes sign with depth. The Love wave trains cannot be fit by the Rayleigh wave model, arriving considerably earlier than predicted by any model consistent with the Rayleigh wave data. The earlier arriving Love waves can be fit if the shear velocity is about 7% faster in the top 80 km than in the Rayleigh wave models (Fig. 3), but the resolution (Fig. 5) of the Love waves is insufficient to discriminate how this polarization anisotropy is distributed between lid and LVZ, and the location of the peak in anisotropy at 50-km depth is not strongly constrained by the data. No anisotropy is required at greater depths, but the limited resolution of the Rayleigh wave data precludes detection of the small velocity differences below 125 km that would be associated with a few percentage of anisotropy.

A polarization anisotropy of 7% is unexpectedly large. SH and SV velocities differ

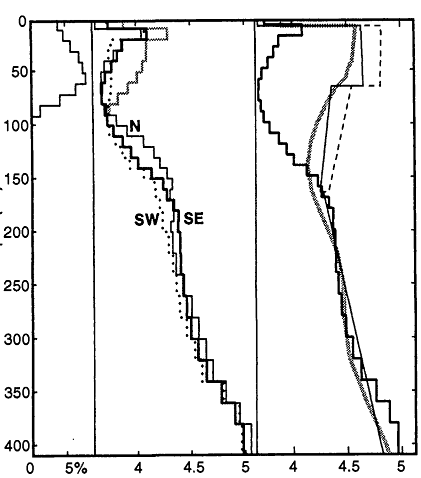

Fig. 3. Shear wave models for the 364/95 event. Three SV (Rayleigh wave) models are shown as solid or dashed lines; one SH (Love wave) model is shown in gray. The percentage of SH-SV anisotropy inferred from one SV model and from the SH model is shown on the left. The SV models are from near-axis OBSs in the northern MELT array (N) and from OBSs on the Nazca (SE) and Pacific plates (SW) from the southern array. The 364 SE model is repeated on the right (heavy line) and shown with a standard isotropic Pacific shear velocity model (*16*) in gray and with the SV (fine line) and SH (dashed line) components of an anisotropic model (*21*).

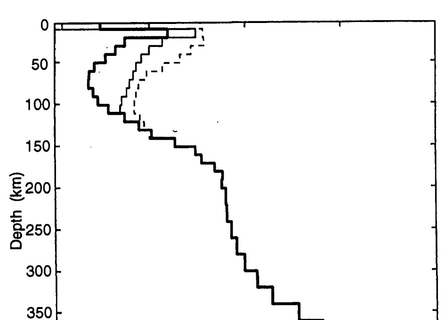

Fig. 4. Best-fitting shear velocity (SV) model for the three events 364/95 (heavy line), 335/95 (fine line), and 345/95 (dashed line). There is a systematic progression in shear velocity with average age of the oceanic crust.

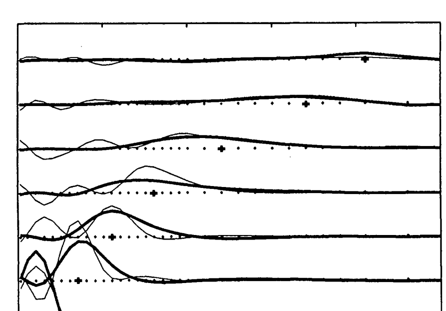

Fig. 5. Resolution kernels for the SV (heavy line) and SH data (fine line) from the 364/95 event showing how a variation in Earth structure at the location of the crosses is mapped into a model.

by up to 4.5% in the upper mantle in the average Earth reference model PREM (*17*), but previous observations of Love and Rayleigh waves across ocean basins indicate that the extent of SH-SV anisotropy decreases near spreading centers (*1*). The extent of anisotropy could be decreased by 1 or 2% by spreading it out over a greater depth range. Two other factors may contribute to exaggerating the difference, but both still require the upper mantle to be anisotropic. First, both Rayleigh and Love waves are expected to be azimuthally anisotropic. The velocity of Rayleigh waves varies as $\cos 2(\theta - \phi)$, where θ is the azimuth of propagation and the fast direction (ϕ) is approximately perpendicular to the ridge (*1, 18*). If this anisotropy is caused by the horizontal alignment of olivine in a shearing flow, then Love wave propagation should be faster on average than would be predicted from a Rayleigh wave model but vary as $\cos 4(\theta - \phi)$, with the fastest direction about 45° from the axis. The oblique ray paths from event 364/95 traveling at an angle of about 25° from the average orientation of the ridge segments may be closer to the slow direction for Rayleigh waves and the fast direction for Love waves. Second, if there is polarization anisotropy, then the lateral gradients in velocity away from the ridge may be different for SH and SV waves, causing the Love and Rayleigh waves to be refracted along substantially different paths. Although the extent of the SH-SV discrepancy may be uncertain because of limited resolution and azimuthal coverage, it is clear that there must be substantial anisotropy distributed throughout much of the upper 100 km.

The velocity models depend on the attenuation in the upper mantle. Fitting the waveforms requires selection of an attenuation model, but because multipathing and focusing also affect the amplitude and phase of arrivals, the constraints on the attenuation model are weak. The vertical dependence of attenuation is poorly resolved for any event, but models that best fit the Rayleigh wave amplitudes for the 364/95 event have high attenuation ($Q_s \approx 50$) in the upper 100 km. This attenuation is greater than that inferred from multiple *S* phases for the upper mantle under the EPR ($Q_s \approx 70$) but less than that suggested for the upper mantle ($Q_s \approx 25$) near the spreading center in the Lau back arc basin (*12, 19*). This attenuation is consistent with the low shear velocities seen in the LVZ and the presence of partial melt. The 335/95 and 345/95 events traveling over progressively older average age crust are best fit with Q_s values of 55 and 90, respectively, consistent with decreasing melt concentrations beneath older oceanic crust.

The two most important findings in this study are the low velocities in the LVZ and the depth to the bottom of the LVZ. Velocities at a depth of 50 km (Fig. 3) are ≈1.0 km/s less than those at the same depth beneath old sea floor (*1*), corresponding to a reduction in shear modulus of nearly 40%. These low velocities must be associated with substantial melt fraction below the rise axis. The actual melt fraction is difficult to assess because it depends strongly on the model of how melt is distributed within the matrix. If the melt were distributed in thin films with an aspect ratio of 0.01, only about 1% by volume would be required, but if the melt is distributed in more equant pockets that more weakly affect the shear velocity, more than 5% melt may be required (*20*).

The velocities in the LVZ are lower than would be expected from the propagation of Rayleigh waves from these and other events across the array (*18*). For example, the model for event 364/95 shown in bold in Fig. 3 predicts that phase velocities at a 25-s period are about 0.2 km/s slower than are observed (*18*). Either the average upper mantle velocities between the earthquake source and the array are substantially lower than in the vicinity of the array, or the event-to-array velocities are biased by our implicit assumption of lateral uniformity in deriving a one-dimensional model. The Rayleigh wave energy may be trapped by a horizontal waveguide formed by a minimum in LVZ velocities and lid thickness near the rise axis, so that the actual ray path is longer than the great circle path. This possibility should be explored in the future.

Low velocities requiring the presence of melt extend to depths of more than 100 km. There is a steep gradient in velocities between about 100 and 180 km. If a discontinuity caused by a sudden onset in melting of upwelling mantle were present, it would be smeared out in our models by lack of resolution and the use of a smoothing criterion in inverting the data. Melting may either increase gradually above 180 km, or there could be a sharp drop in velocity and increase in melt concentration where the gradient is steepest, from depths of 130 to 160 km. We require no anomaly below 200-km depth.

Our models predict that one-way travel times for vertically propagating *S* waves beneath the ridge axis differ by more than 4 s from travel times through standard models for older sea floor (*16, 21*) just because of the structure shallower than 200 km. Previous observations (*22*) of the seismic *SS* phase reflecting beneath the EPR found two-way delays of about 5 s compared with old sea floor. The large amplitude of this anomaly was cited as evidence that mid-ocean ridge shear velocity anomalies must extend to a depth of at least 300 km (*23*), but our results show that the delay can be explained entirely by a structure shallower than 200 km.

REFERENCES AND NOTES

1. C. E. Nishimura and D. W. Forsyth, *Geophys. J. Int.* **96**, 203 (1989).
2. Y. S. Zhang and T. Lay, *J. Geophys. Res.* **101**, 8415 (1996).
3. G. Ekstrom, J. Tromp, E. W. F. Larson, *ibid.* **102**, 8137 (1997).
4. B. Romanowicz, *Annu. Rev. Earth Planet. Sci.* **19**, 77 (1991).
5. The horizontal component data were rotated into radial (corresponding to the Rayleigh wave) and tangential (corresponding to the Love wave) components with instrument orientations determined from short-period *P*-wave polarizations. All transverse records used in the analysis have SNRs exceeding 12 dB (peak-to-peak noise over minimum body wave peak-to-peak amplitude). Vertical component records have SNRs exceeding 16 dB.
6. The compressional velocity α was assumed to be isotropic and equal to 1.81 times the SV component of the shear velocity. The modeling of SV or SH structure is quite insensitive to α or density, but there is minor sensitivity to *P*-wave anisotropy.
7. J. Park, *Geophys. J. Int.* **126**, 173 (1996).
8. ——— and Y. Yu, *Science* **261**, 1159 (1993).
9. G. E. Randall, *Geophys. J. Int.* **118**, 245 (1994). X. Yu modified the code, adding a water layer.
10. W. Friederich, E. Wielandt, S. Strange, *ibid.* **119**, 931 (1994).
11. The data and synthetic data were identically filtered with a passband from 0.008 to 0.06 Hz. The low-frequency limit was set by noise limitations. For the SH data, the high-pass corner was moved to 0.017 Hz (60 s) because of high long-period noise levels. It is more usual to model either displacement or velocity waveforms, so we experimented by integrating both the data and synthetic time series once or twice to approximate either velocity or displacement. Integrating twice strongly degraded the inversion process because of high long-period noise levels. There was no obvious advantage to modeling velocity.
12. Y. Xu and D. A. Wiens, *J. Geophys. Res.* **102**, 27439 (1997). We investigated a large range of starting models to ensure that the final results represented the best-fitting model in a global rather than a local sense. The final models were only subtly dependent on the starting models.
13. D. L. Anderson and A. M. Dziewonski, *Geophys. J. R. Astron. Soc.* **69**, 383 (1982).
14. D. Zhao *et al.*, *Science* **278**, 254 (1997).
15. J. J. Leveque, M. Cara, D. Rouland, *Geophys. J. Int.* **104**, 565 (1991).
16. M. Cara, *Geophys. J. R. Astron. Soc.* **57**, 649 (1979).
17. A. Dziewonski and J. Woodhouse, *J. Geophys. Res.* **88**, 3247 (1983).
18. D. W. Forsyth, S. C. Webb, L. M. Dorman, Y. Shen, *Science* **280**, 1235 (1998).
19. X.-Y. Ding and S. P. Grand, *J. Geophys. Res.* **98**, 1973 (1993).
20. D. W. Forsyth, in *Mantle Flow and Melt Generation at Mid Ocean Ridges*, J. Phipps Morgan, D. K. Blackman, J. Sinton, Eds. (American Geophysical Union, Washington, DC, 1992), pp. 1–65.
21. J. B. Gaherty, T. H. Jordan, L. S. Gee, *J. Geophys. Res.* **101**, 22291 (1996).
22. R. L. Woodward and G. Masters, *ibid.* **96**, 6351 (1991).
23. W.-J. Su, R. L. Anderson, A. M. Dziewonski, *Nature* **360**, 149 (1992).

24. This project was funded by the NSF as part of the Ridge Inter-Disciplinary Global Experiment program. We thank G. E. Randall and Y. Xu for the use of their codes, B. D. Cornuelle for help with programming the inversion, W. C. Crawford and C. E. Golden for help at sea, and G. R. Lada for work on the data.

18 February 1998; accepted 23 April 1998